

On the hadronic origin of the TeV radiation from GRB 190114C

Silvia Gagliardini^{a, b, *}, Silvia Celli^{a, b}, Dafne Guetta^c, Angela Zegarelli^{a, b},

Antonio Capone^{b, c}, Stefano Campion^{a, b}, and Irene Di Palma^{a, b}

^a *Dipartimento di Fisica dell'Università La Sapienza, P. le Aldo Moro 2, I-00185 Rome, Italy,*

^b *Istituto Nazionale di Fisica Nucleare, Sezione di Roma, P. le Aldo Moro 2, I-00185 Rome, Italy,*

^c *Department of Physics, Ariel University, Ariel, Israel*

The recently discovered TeV emission from Gamma-Ray Bursts (GRBs) hints towards a possible hadronic origin of this radiation component. We developed a Monte Carlo (MC) simulation reproducing the kinematics of photo-hadronic interactions at internal shocks, including the pair production process that the secondary gamma rays undergo in the GRB jet. We find that sub-TeV observations of GRB 190114C can be reproduced by a baryonic energy content comparable to that in sub-GeV photons and a bulk Lorentz factor $\Gamma = 100$, with a ms variability timescale. Neutrino flux predictions by the model are found to be consistent with experimental upper limits set by ANTARES and IceCube.

I. INTRODUCTION

The detection of GRBs in sub-TeV gamma rays has disclosed a new window of the electromagnetic spectrum for studying mildly relativistic outflows at the highest energies. GRB 190114C is the first long-duration GRB reported in the TeV band by the Major Atmospheric Gamma Imaging Cherenkov (MAGIC) telescopes. High-energy gamma rays (0.2–1 TeV) were detected by the instrument with high significance [1], during both the prompt and afterglow phases of the GRB emission. The sub-TeV radiation component has a power comparable to that of the sub-GeV one, attributed to the synchrotron process. Therefore, sub-TeV emission has been interpreted as due to leptonic processes [2], usually considered responsible for gamma ray production in GRBs. However, a purely leptonic scenario consisting of synchrotron self-Compton radiation produced at external shocks has been shown to not match the broadband emission observed in GRB 190114C [2]. In addition, the large number of parameters involved in the model highly limits its prediction power. Although firm conclusions on the production mechanisms of GeV-TeV emission have been reached so far [3–9], the hypothesis that part of this emission might be caused by the presence of a hadronic component cannot be excluded. Several authors [4, 6, 7] have hence explored the possibility that processes involving photo-meson interactions might play a relevant role in the formation of the gamma-ray spectrum of GRB 190114C up to TeV energies. Since the dissipation mechanism responsible for the acceleration of electrons could be invoked for the acceleration of protons, high-energy neutrinos are also expected [10–13].

In this paper, we test a scenario in which the very high energy (VHE) emission of GRB 190114C is due to photo-hadronic interactions occurring in the GRB jet during the so-called prompt phase. To this extent, we consider the standard fireball model in which, within the

relativistic outflow of the jet, energy dissipation occurs at shocks internally to the jet or through interactions with ambient matter [10, 11]. Thus, a substantial part of the bulk kinetic energy is converted into internal energy, which is then distributed between electrons, protons, and the magnetic field. The internally accelerated electrons are presumably responsible for the keV–GeV photons observed in the GRB, which are emitted through synchrotron or inverse Compton processes. Accelerated protons may interact with these photons (\sim MeV) and produce both neutral and charged pions, which in turn decay, originating respectively high-energy photons and neutrinos.

The paper is structured as follows: in Sec. II we introduce the spectral and temporal properties of GRB 190114C. In Sec. III we present our MC simulation, developed to describe the physics of photo-hadronic interactions occurring in the internal shock (IS) region of the GRB jet. In Sec. IV we compare the photon flux resulting from our simulation to the Extragalactic Background Light (EBL) deconvolved MAGIC data, obtaining a set of best fit values of the model parameters. From the same simulation we predict a flux of high energy neutrinos and we evaluate the expected number of events in present and future experiments. A discussion of the results is provided in Sec. V, where conclusions are ultimately derived.

II. GRB 190114C: SPECTRAL AND TEMPORAL PROPERTIES

GRB 190114C was the first GRB detected at sub-TeV energies, among the few observed so far. The combination of a rapid follow-up by MAGIC [14] with the rather contained distance of the source (confirmed from its optical counterpart to be at redshift $z = 0.4245$ [15, 16]), in terms of extra-galactic scales, has allowed to unveil the presence of an extremely energetic radiation component in GRBs, long before theorised [17]. A wealth of observations has allowed for the precise characterisation of the temporal and spectral features of this source. In the

* silvia.gagliardini@roma1.infn.it

gamma-ray band, starting from the triggering instrument Swift [18], further observations have followed by GBM [19] and LAT [20] onboard of the *Fermi* satellite (up to 22.9 GeV), AGILE/MCAL [21], Integral/SPI-ACS [22] and Konus-Wind [23].

The prompt phase of GRB 190114C, as observed by Fermi-GBM, appears as a multi-peak emission lasting $T_{90} \simeq 116$ s (50-300 keV), being T_{90} the duration where 90% of the gamma-ray fluence was detected. The time-averaged spectrum in the first ~ 40 s can be described by a Band function with low and high-energy slopes equal to $\alpha = 1.058$ and $\beta = 3.18$, respectively, and a break energy value of $E_b \simeq 1.1$ MeV in the observed frame [19], and a gamma-ray fluence of $F_\gamma = 3.99 \times 10^{-4}$ erg cm $^{-2}$ (10-1000 keV). As such, the isotropic energy release in the source frame amounts to $E_{\text{iso}} \simeq 3 \times 10^{53}$ erg, indicating a fairly energetic (though not the most extreme) GRB. In turn, MAGIC reported a first detection starting from 68 s after the Fermi-GBM trigger with a significance above 50σ : VHE emission lasted for ~ 40 minutes, with the highest photon energy observed amounting to $E_{\text{max}} = 0.852$ TeV [1]. Within this extended temporal window, time-dependent analysis of VHE data was also performed, showing a systematical decrease in flux normalization as well as a steepening trend over time. The earliest high-energy photon spectrum reported by MAGIC refers to the time interval 68-110 s, that entirely overlaps with the T_{90} estimated by Fermi-GBM for the prompt emission. During this time interval, the intrinsic burst spectrum in the 0.2-1 TeV band is characterised by a pure power-law ($\propto E^{-\xi}$) with $\xi = 2.16_{-0.31}^{+0.29}$ [2]. The photon spectral slope at the source has been derived taking into account the severe attenuation of the gamma-ray flux due to its propagation to the Earth within the EBL [2], according to the Dominguez et al. model [24]. We hence consider such an intrinsic spectrum and we compare it with the prediction of the gamma-ray flux emerging from our simulation of the IS region.

Additionally, we have investigated the effects of adopting a different EBL model, e.g. that from Franceschini et al. [25, 26], finding results consistent with the Dominguez et al. model within the statistical uncertainty of the MAGIC measurements.

The temporal overlap between the MAGIC observations and T_{90} is not sufficient to definitely attribute the high-energy photons measured by MAGIC to the prompt or to the afterglow phase of the GRB emission. In this work, we consider a scenario where the observed TeV emission can be ascribed to the prompt phase, in particular to radiation emerging from hadronic interactions occurring at the IS region between accelerated protons and the Band-like target radiation field. The two main features of a hadronic scenario are the bulk Lorentz factor Γ , and the amount of energy channeled into relativistic protons $E_{\text{iso,p}}$. The latter can be expressed with the baryon loading f_p defined as $f_p = E_{\text{iso,p}}/E_{\text{iso}}$. Both the values

of Γ and f_p can be constrained in order to reproduce the VHE spectrum in terms of hadronic gamma rays. Concerning the value of Γ , we estimate the minimum Lorentz factor required by a $E_\gamma \simeq 1$ MeV photon to be revealed at Earth, as observed by Fermi-GBM. This can be constrained by requiring that the optical thickness τ for pair production $\gamma\gamma \rightarrow e^+e^-$ has to be $\tau \leq 1$. Following Eq. (5) of [27], we computed the total number of photons emitted during the first ~ 40 s, with energy greater than $E_{\text{max,pair}} = (2\Gamma m_e c^2)^2/E_\gamma$, for different variability times $t_{\text{var}} = 6, 3, 1$ ms [28], obtaining minimum Lorentz factor values $\Gamma_{\text{min}} \simeq 60, 70, 90$ respectively.

III. MONTE CARLO SIMULATION

Modelling the physical processes occurring inside the IS region of the expanding GRB fireball requires the characterisation of the site where particles propagation and interactions take place. We here consider a simplified one-zone scenario, similarly to e.g. [29-31], in which mildly relativistic shells of plasma collide at a typical radius [32]

$$R_{\text{IS}} = \frac{2\Gamma^2 ct_{\text{var}}}{(1+z)} \simeq 4 \times 10^{12} \left(\frac{\Gamma}{100} \right)^2 \left(\frac{t_{\text{var}}}{0.01 \text{ s}} \right) \left(\frac{1.4}{1+z} \right) \text{ cm}, \quad (1)$$

whose value is related to Γ and to the variability time t_{var} . In our simulation, we assume for the variability timescale values ranging from 1 to 6 ms, the latter being suggested by observations performed during the prompt phase of GRB 190114C [28]. In turn, the Γ factor is treated as a free parameter of the model, whose most likely value will be fixed as the one that best reproduces MAGIC data. The MC calculation is performed in the IS frame, where a spherical geometry is assumed [33]. The total fluence is assumed to be coming from N interaction regions, where $N = T_{90}/t_{\text{var}}$. The shell width, in the IS frame, is given by $\Delta R_{\text{IS}} = N\Gamma ct_{\text{var}}/(1+z)$. The process relies on the generation of accelerated protons, with energy range $1 - 10^9$ GeV, characterised by a differential energy spectrum according to $dN_p/dE_p \propto E_p^{-2}$. The target photon energy distribution in the IS frame is assumed to reproduce the Band function observed by Fermi-GBM [19] in the prompt phase of the GRB, eventually extended to high energy, in order to allow Δ production with the entire spectrum of accelerated protons. Once generated, a proton can either interact with ambient photons if the center of mass energy is above the interaction threshold condition or propagate further in the shell. The interaction length $\lambda_{p\gamma}(s) = [n_\gamma \sigma_{p\gamma}(s)]^{-1}$ is evaluated, depending on the $p\gamma$ center of mass energy, and on the density of photons in the IS frame $n_\gamma(\epsilon_{\text{th},\Delta}^{\text{IS}})$ allowing a center of mass energy above the Δ production, namely such that $\epsilon_{\text{th},\Delta}^{\text{IS}} = (m_\Delta^2 - m_p^2)c^4/(4E_p^{\text{IS}})$, (m_Δ and m_p being respectively the Δ^+ and proton masses). A mean free path x_p is assigned to each proton, following a procedure analogous to that described in [34]: if $x_p < R_{\text{IS}}$ and if the

threshold condition for the Δ^+ production is satisfied, the photo-meson interaction occurs. The energies of protons (E_p^{IS}) and photons ($\epsilon_\gamma^{\text{IS}}$) that satisfy the photo-meson production condition are shown in Fig. 1. The multi-

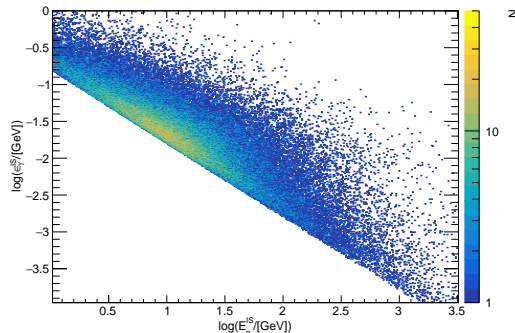


FIG. 1. Distribution of simulated events exceeding the photo-meson threshold in the IS frame ($\Gamma = 100$ and $t_{\text{var}} = 1$ ms): the x-axis refers to accelerated proton energies, while the y-axis refers to target photon energies.

pion generation beyond the resonant Δ^+ production is also simulated. Particles like π^0 , π^\pm , μ^\pm , ν_μ , $\bar{\nu}_\mu$, ν_e , $\bar{\nu}_e$, as well as secondary protons originated by the interaction, are followed by the simulation. The secondary protons are tracked until they leave the IS region as to account for possible reinteractions along their path with the same target photon spectrum. Pions and muons are followed until they decay.

To account for energy losses of charged particles within the propagation timescale inside the IS region, we introduce purely exponential spectral cut-offs. In particular, the steady state energy distribution for protons is obtained by comparing the acceleration timescale $t_{\text{acc}}(E_p^{\text{IS}}) = r_L(E_p^{\text{IS}})/c$, being r_L the particle Larmor radius, to the average inelastic collision timescale for the Δ -baryon production $t_{p\gamma}(E_p^{\text{IS}}) = [n_\gamma(\epsilon_{\text{th},\Delta}^{\text{IS}})c\sigma_{p\gamma}^\Delta K_{p\gamma}]^{-1}$. In the previous expression, $K_{p\gamma} = 0.13$ and $\sigma_{p\gamma}^\Delta = 5 \times 10^{-28} \text{ cm}^2$ are respectively the inelasticity and the cross section of the interaction at the threshold [35]. Other energy-loss processes, such as adiabatic and synchrotron losses, have negligible impact on protons. As a reference, for $\Gamma = 100$ and $t_{\text{var}} = 1$ ms we find that the proton cut-off energy amounts to $E_{p,\text{cut}}^{\text{IS}} \simeq 2.4$ PeV.

Muons and charged pions could be affected by synchrotron losses. To account for this effect, we evaluated the magnetic field value at IS by equating the magnetic energy density $U_B = B^2/(8\pi)$ to the kinetic energy density of the accelerated electrons. Naming ϵ_B the fraction of the jet energy converted into magnetic energy, and ϵ_e the fraction of the jet energy carried by the electrons, later entirely transferred to the photons adopted as the proton target, our assumption is $\epsilon_e = \epsilon_B$. Pion and muon lifetimes are found to be longer than the synchrotron timescale $t_{\text{syn}}(E^{\text{IS}}) = 9m^4/(4cq_e^4 E^{\text{IS}} B^2)$ for IS energies, respectively, above $E_{\mu^\pm,\text{cut}}^{\text{IS}} \simeq 0.5$ TeV and

$$E_{\pi^\pm,\text{cut}}^{\text{IS}} \simeq 9 \text{ TeV} \quad (\Gamma = 100, t_{\text{var}} = 1 \text{ ms}).$$

The kinematics of $p\gamma$ interactions follows the methods outlined in [34]. The energy particle distribution for interacting protons, charged pions, muons, and neutrinos is shown in Fig. 2. The simulation is performed in the IS assuming $\Gamma = 100$ and $t_{\text{var}} = 1$ ms.

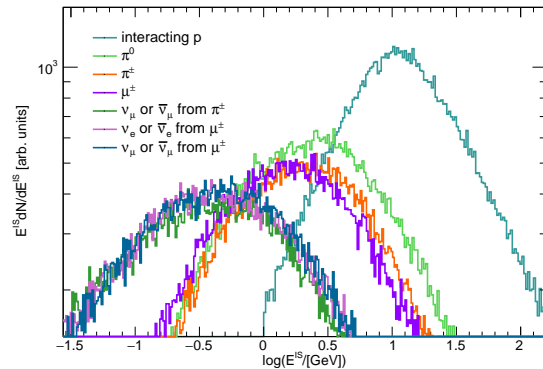


FIG. 2. Particle spectra resulting from $p\gamma$ interactions, obtained in the IS frame from the simulation with $\Gamma = 100$ and $t_{\text{var}} = 1$ ms. Protons that have emerged from the first interaction are also shown, though they might further interact in the following.

Concerning the neutral pion production and decay, we consider the possibility that each originated gamma ray might further interact within the IS shell with low energy ambient photons, via e^\pm pair production. The radiation length of this process is evaluated as $\lambda_{\gamma\gamma}(s') = [n_\gamma(\epsilon_{\text{th},e^\pm}^{\text{IS}})\sigma_{\gamma\gamma}(s')]^{-1}$, where s' is the $\gamma\gamma$ center of mass energy squared, $\sigma_{\gamma\gamma}$ is the e^\pm pair production cross section [36], and $\epsilon_{\text{th},e^\pm}^{\text{IS}}$ is the target photon threshold energy. The target photon is extracted from a uniformly distributed $\cos\theta$ angle with respect to the gamma ray. For each gamma with energy E_γ^{IS} originated from π^0 decay, we extract its mean free path x_γ according to the radiation length $\lambda_{\gamma\gamma}$, and if $x_\gamma < R_{\text{IS}}$, we evaluate whether or not the e^\pm pair production threshold condition is satisfied [36]:

$$E_\gamma^{\text{IS}} \geq \frac{2m_e^2 c^4}{\epsilon^{\text{IS}}(1 - \cos\theta)} \simeq \frac{1.02}{\epsilon_{\text{eV}}^{\text{IS}}(1 - \cos\theta)} \text{ TeV}. \quad (2)$$

For the purposes of our simulation, the Band spectrum of target photons is assumed to extend outside of the Fermi-GBM observed energy range, by about three decades, as to allow the pair production to occur with the gamma ray originated from π^0 -decay. As a result of our computation, we find the fraction of absorbed high energy photons amounts to $\simeq 60\%$ for 10 GeV gamma rays in the IS frame ($\Gamma = 100$ and $t_{\text{var}} = 1$ ms). This fraction increases for more energetic gamma rays. We observe that, at fixed gamma-ray energy, the effect of $\gamma\gamma$ absorption results larger for lower values of Γ , since the target photon density increases lowering the bulk Lorentz factor.

The gamma rays surviving the e^\pm production process in the IS shell will emerge from this region and would eventually be observed in the laboratory frame with energy $E_{\text{obs}} = \Gamma E_{\text{IS}}/(1+z)$. Such photons can be directly compared with the intrinsic Spectral Energy Density (SED) derived by MAGIC.

IV. RESULTS: GAMMA RAYS AND NEUTRINOS FROM PHOTO-HADRONIC INTERACTIONS

We perform MC simulation for different values of t_{var} and Γ , obtaining spectra of high-energy gamma rays and neutrinos emerging from the interaction region. We then convert these spectra into expected fluxes on Earth by taking into account the cosmological nature of GRBs. For the particle energy flux $E^2\phi(E)$, either photons or neutrinos, we rescaled the IS energy spectrum through: i) the comoving distance $d_c = d_L/(1+z)$, where d_L represents the luminosity distance, ii) the first time interval of MAGIC observations $\Delta t = 42$ s, and iii) the energy conversion factor from the IS to the observed frame, as:

$$E^2\phi(E) = f_p \Gamma \frac{(1+z)}{4\pi d_L^2 \Delta t} \left(E^2 \frac{dN}{dE} \right)_{\text{IS}}. \quad (3)$$

For each simulated Γ and t_{var} set of values, the baryon loading f_p has been varied in the interval $0.1 - 5.0$ in uniform steps of width $\Delta f_p = 0.1$, in order to derive the best agreement between the EBL-deconvolved MAGIC data in the 68-110 s time interval [2] and the simulated fluxes, through a χ^2 statistical test. Considering the minimum bulk Lorentz factor values dictated by the opacity argument and derived in Sec. II, we obtain the following set of best-fit parameters: for the case $t_{\text{var}} = 6$ ms, we find $\Gamma = 70$ and $f_p = 0.95$; in turn, for $t_{\text{var}} = 3$ ms, we obtain $\Gamma = 80$ and $f_p = 0.93$; finally, for $t_{\text{var}} = 1$ ms, we derive $\Gamma = 100$ and $f_p = 1.1$. Remarkably, despite the broad variation in the values of bulk Lorentz factor that characterize the models possibly reproducing sub-TeV data, an almost constant f_p is obtained, suggesting a comparable amount of energy being channeled in the hadronic and leptonic jet components. By fixing Γ to the best-fit value, we evaluated the statistical uncertainty on flux normalisation. This result is shown in Figure 3, where the modellings that best reproduce the EBL-deconvolved MAGIC data are reported on top of it, the shaded area representing the 1σ statistical uncertainty evaluated over f_p .

A direct proof of the hadronic origin of the observed TeV radiation might come from coincident neutrino observations. Because of the transient nature of GRBs, the detection of a single neutrino event would allow to identify these sources as extreme hadronic accelerators. Despite the experimental efforts, no clear signal has emerged so far in data from the ANTARES and IceCube telescopes [37] [38], when searching for spatial and temporal coincidences with the prompt emission of GRBs. This

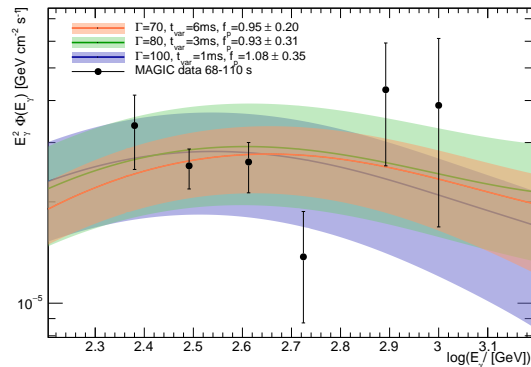


FIG. 3. Comparison between the EBL-deconvolved flux of GRB 190114C, as measured by MAGIC in the temporal interval 68-110 s [2], and the simulated photon flux arising from the π^0 -decay, after accounting for internal gamma-ray absorption. Different parameter values of the model are tested, as indicated in the legend.

leads to a constraint on the possible contribution of standard GRBs to less than 10% of the diffuse cosmic neutrino flux [39–42]. Additionally, it is still unclear whether TeV-emitting GRBs behave as the standard GRB population: consequently, it appears of paramount importance to investigate neutrino emissions from this newly discovered class of sources. Both the ANTARES and IceCube Collaborations have searched for coincident neutrino-induced signals from the direction of GRB 190114C. No events were observed in extended time windows, covering both the prompt and the afterglow phase of the GRB, leading to upper limits on the expected neutrino fluence. In the case of ANTARES, the 90% confidence level integrated limit amounts to $1.6 \text{ GeV}/\text{cm}^2$, while for IceCube it amounts to $0.44 \text{ GeV}/\text{cm}^2$ [43, 44]. In both cases, the constraints are limited to the muon neutrino component reaching Earth. In fact, because angular precision is a crucial feature to reduce the atmospheric background entering the search cone angle, muon neutrino charged-current interactions constitute the better astronomical channel, as muons emerge from these, which can be identified in large volume neutrino telescopes as long tracks. Neutrino fluxes arriving on Earth differ from those produced at source due to the effect of leptonic flavor mixing: hence, in order to have a direct comparison between the experimental upper limits and the predictions from the hadronic modelling here developed, neutrino oscillations have to be accounted for. By considering the normal ordering case in the standard three-flavour scenario [45], we obtain the neutrino energy flux on Earth, which is shown for muon neutrinos and antineutrinos in Fig. 4. Current neutrino detectors ANTARES and IceCube have investigated their data looking for possible spatially coincident neutrino signals, however the resulting upper limits are a few order of magnitudes above the model predictions here presented, indicating that the non-detection of cur-

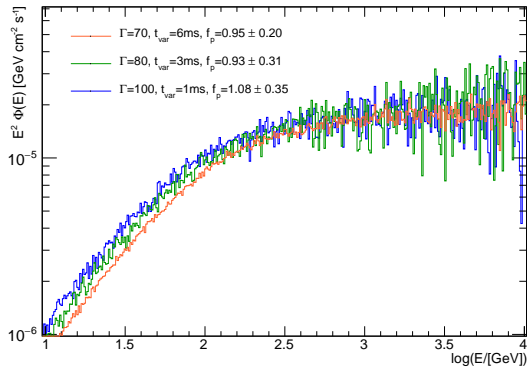


FIG. 4. Muon neutrino and antineutrino fluxes expected on Earth from GRB 190114C, obtained from the simulations in the time interval 68-110 s for different model parameter values, as indicated in the legend.

rent instruments is compatible with the hadronic model expectations for the values of f_p and Γ that better reproduce the sub-TeV gamma-ray MAGIC data. To understand whether future neutrino detectors, as the full configuration of KM3NeT, might be able to uncover a level of signal comparable to that expected from GRB 190114C, we first obtain the muon neutrino (and antineutrino) fluence $dN_{\nu_\mu}/(dE_{\nu_\mu} dS)$, and then compute the expected number of track-like events as

$$N_{\text{events}}(\delta) = \int A_{\text{eff}}^{\nu_\mu}(E_\nu, \delta) \left(\frac{dN_{\nu_\mu}}{dE_{\nu_\mu} dS} \right)_{\text{Earth}} dE_{\nu_\mu}, \quad (4)$$

where the neutrino telescope effective area $A_{\text{eff}}^{\nu_\mu}$ is a function of the neutrino energy and of the source declination δ . For the purpose of the computation, the public effective areas of ANTARES, IceCube and KM3NeT are adopted, averaged over neutrinos and antineutrinos. In the case of ANTARES, we consider the declination band $-45^\circ < \delta < 0^\circ$ [37] including the position of GRB 190114C, in the case of IceCube instead the effective area refers to the band $-30^\circ < \delta < 0^\circ$ [38], while for KM3NeT we adopt mean values of the high-energy detector ARCA (averaged over the entire sky) [46]. It is also worth to note that, while the ANTARES and IceCube have been released at the analysis level for point source studies, the KM3NeT/ARCA one is at trigger level. We provide in the following the expected number of neutrino-induced events in the three large-volume detectors, as reported in Table I relatively to the simulation with $t_{\text{var}} = 1$ ms, $\Gamma = 100$ and $f_p = 1.1$. Even though the coincident background rate due to atmospheric neutrinos is by orders of magnitude lower than the signal rate expected from a source like GRB 190114C, a detection from a single GRB appears to be very difficult. This result suggests that stacking several GRBs of the same kind could be the only viable solution for a significant detection.

Detector	Declination band	N_{events}
ANTARES	$-45^\circ < \delta < 0^\circ$	1×10^{-3}
IceCube	$-30^\circ < \delta < 0^\circ$	2×10^{-2}
KM3NeT/ARCA	Average	1×10^{-1}

TABLE I. Signal events expected in different neutrino telescopes, as induced by ν_μ interactions during the [68;100] s time interval of the prompt emission of GRB 190114C, for the model with $t_{\text{var}} = 1$ ms, $\Gamma = 100$ and $f_p = 1.1$. The computations refer to instrument effective areas in the declination band including the source location (ANTARES [37], IceCube [38], and KM3NeT [46]).

V. DISCUSSION AND CONCLUSIONS

The successful observation of radiation from GRBs extending up to the TeV domain has provided further evidence of the extreme nature of these sources. However, there is still poor understanding of the processes that characterize the observed TeV emission emerging from GRB 190114C (and the few other GRBs detected at TeV energies). The newly discovered radiation component might witness the presence of effective hadronic acceleration in the jet of the burst, possibly already during the prompt phase of the emission. This occurrence would establish the connection between GRBs and Ultra-High-Energy Cosmic Rays (UHECRs), which remains a long-standing paradigm still to be proven. To test the hypothesis of the hadronic origin of TeV radiation, we developed a MC simulation of photo-meson interactions between high-energy protons and target photons distributed according to a Band-like spectrum, as indicated by Fermi-GBM observations. After computing the spectra of secondary particles emerging from these interactions, we additionally simulated the electromagnetic absorption that gamma rays undergo in the IS shell. The spectrum of escaping photons thus obtained has been compared to the intrinsic source spectrum derived by deconvolving MAGIC observations of GRB 190114C in the EBL. The free parameters of the hadronic model have thus been constrained by means of a residual minimisation procedure, indicating that the source channelled a comparable amount of energy into photons and hadrons. Extended studies about the entire sample of observed TeV GRBs are required to understand the physical mechanisms responsible for the TeV emission. In particular, it appears to crucial to have a better characterization of the very-high-energy photon spectrum in the early stages of the GRB emission, which seems to be currently limited by the prompt response of imaging atmospheric Cherenkov telescopes in pointing. Confirmation of the hadronic origin of sub-TeV radiation might, in principle, arise from neutrino observations. In the context of the parameters that better reproduce MAGIC data, however, such a detection from GRB 190114C appears extremely unrealistic, as confirmed by the lack of spatial correlations in data from both the ANTARES and IceCube neutrino telescopes.

ACKNOWLEDGMENTS

The authors acknowledge the support of the Amaldi Research Center funded by the MIUR programme “Dipartimento di Eccellenza” (CUP:B81I18001170001),

the Sapienza School for Advanced Studies (SSAS) and the support of the Sapienza Grants No. RM120172AEF49A82 and RG12117A87956C66. The authors are thankful to Enrico Peretti for fruitful discussions on the manuscript content.

-
- [1] V. A. Acciari et al. (MAGIC Collaboration), *Nature* 575 (2019) 455
- [2] V. A. Acciari et al. (MAGIC Collaboration), *Nature* 575 (2019) 459
- [3] M. E. Ravasio, G. Oganessian, O. S. Salafia, G. Ghirlanda, G. Ghisellini, M. Branchesi, S. Campana, S. Covino & R. Salvaterra, *A&A* 626 (2019) 12
- [4] N. Fraija, R. Barniol Duran, S. Dichiaro & P. Beniamini, *ApJ* 883 (2019b) 162
- [5] X. Y. Wang, R. Y. Liu, H. M. Zhang, S. Q. Xi and B. Zhang, *ApJ* 884 (2019) 117
- [6] E. Derishev & T. Piran, *ApJ*, 880 (2019) 27
- [7] S. Sahu, & C. E. López Fortín, *ApJ* 895 (2020) 41
- [8] V. Chand, P. S. Pal, A. Banerjee, V. Sharma, P. H. T. Tam, and X. He, *ApJ* 903 (2020) 9
- [9] J. A. Rueda, R. Ruffini, M. Karlica, R. Moradi & Y. Wang, *ApJ* 893 (2020) 148
- [10] D. Eichler, D. Guetta & M. Pohl, *ApJ* 722 (2010) 543
- [11] D. Guetta, M. Spada & E. Waxman, *ApJ* 559 (2001) 101
- [12] D. Guetta, *JHEAp*, 7, 90 (2015)
- [13] L. Yacobi, D. Guetta & E. Behar, *ApJ* 793 (2014) 48
- [14] R. Mirzoyan et al., *ATel* 12390 (2019) 1
- [15] J. Selsing et al. (NOT Collaboration) *GCN* 23695 (2019)
- [16] A. J. Castro-Tirado et al. (GTC Collaboration) *GCN* 23708 (2019)
- [17] E. V. Derishev, V. V. Kocharovskiy & V. V. Kocharovskya, *Advances in Space Research (ASR)* 27 (2001) 813-818
- [18] J. D. Gropp et al. (Swift Collaboration) *GCN* 23688 (2019)
- [19] R. Hamburg et al. (Fermi-GBM Collaboration), 2019, *GCN* 23707
- [20] D. Kocevski et al. (Fermi-LAT Collaboration), 2019, *GCN* 23709
- [21] A. Ursi et al. (AGILE Collaboration), *GCN* 23712 (2019)
- [22] P. Minaev & A. Pozanenko, *GCN* 23714 (2019)
- [23] D. Frederiks et al. (Konus-Wind Collaboration), *GCN* 23737 (2019)
- [24] A. Dominguez et al., *Mon. Not. R. Astron. Soc.* 41 (2011) 2556–2578
- [25] A. Franceschini & G. Rodighiero, *A&A* 603 (2017) A34
- [26] A. Franceschini & G. Rodighiero, *A&A* 614 (2018) C1
- [27] Y. Lithwick & R. Sari, *The Astrophysical Journal* 555 (2001) 1
- [28] M. Ajello et al., *ApJ* 890 (2020) 9
- [29] K. Murase & S. Nagataki, *Phys. Rev. D* 73 (2006) 063002
- [30] K. Asano, S. Inoue & P. Meszaros, *Astrophysical Journal* 699 (2009) 953
- [31] S. Hummer, P. Baerwald & W. Winter, *Phys. Rev. Lett.* 108 (2012) 231101
- [32] P. Baerwald, M. Bustamante, K. Murase & W. Winter, *Nat. Commun.* 6 (2015) 6783
- [33] P. Baerwald, S. Hummer & W. Winter, *arXiv:1107.5583v3 [astro-ph.HE]* 13 Apr 2012
- [34] M. Fasano, S. Celli, D. Guetta, A. Capone, A. Zegarelli & I. Di Palma, *JCAP* 09 (2021) 044
- [35] A. Atoyan & C.D. Dermer, *Phys. Rev. Lett.* 87 (2001) 221102
- [36] S. Vernetto and P. Lipari, *Phys. Rev. D* 94 (2016) 063009
- [37] S. Adrian-Martínez et al. (ANTARES Collaboration), *Astrophys. J.* 760 (2012) 53
- [38] M. G. Aartsen et al. (IceCube Collaboration), *Astrophys. J.* 796 (2014) 109
- [39] S. Adrian-Martínez et al. (ANTARES Collaboration), *Astron. Astrophys.* 559 (2013) A9
- [40] A. Albert et al. (ANTARES Collaboration), *Mon. Not. R. Astron. Soc.* 469 (2017) 906
- [41] A. Albert et al. (ANTARES Collaboration), *Mon. Not. R. Astron. Soc.* 500 (2021) 5614
- [42] M. G. Aartsen et al. (IceCube Collaboration), *Astrophys. J.* 843 (2017) 112
- [43] A. Albert et al. (ANTARES Collaboration), *JCAP* 03 (2021) 092
- [44] J. Vandenbroucke et al. (IceCube Collaboration), *ATel* 12395 (2019)
- [45] C. Mascaretti & F. Vissani, *JCAP* 08 (2019) 004
- [46] S. Adrian-Martínez et al. (KM3NeT Collaboration), *J. Phys. G: Nucl. Part. Phys.* 43 (2016) 084001